Analytical Methods

PAPER

View Article Online
View Journal | View Issue

Cite this: *Anal. Methods*, 2016, **8**, 2936

Binding affinity analysis of the interaction between Homer EVH domain and ryanodine receptor with biosensors based on imaging ellipsometry

Tengfei Kang,[abc] Kaiming Zhang,[d] Changcheng Yin,[d] Yu Niu*[ab] and Gang Jin*[ab]

Received 11th January 2016
Accepted 7th March 2016

DOI: 10.1039/c6ay00089d

www.rsc.org/methods

The interaction between the Homer EVH domain and RyR plays an important role in calcium signaling channels in the heart and the skeletal muscles. A biosensor based on imaging ellipsometry was used to analyze the binding affinity between the Homer EVH domain and RyR. The results confirm that the Homer EVH domain can recognize RyR specifically with high binding affinity of approximately 10^{-8} M. This information will contribute to understanding of the role of the interaction between the Homer EVH domain and RyR in intracellular calcium channels.

Introduction

The ryanodine receptors (RyRs) of intracellular calcium channels play a crucial role in the calcium release process in different signaling pathways.[1–3] In the heart and skeletal muscles, regulation of RyR-dependent calcium channels involves the Homer protein family.[4–6] The enabled/vasodilator-stimulated phospho protein homology (EVH) domain, a highly conserved sequence in all members of the Homer protein family, binds selectively to proline-rich motifs of RyRs,[7–9] forming complexes that enhance calcium release. Although much effort has been directed at exploration of the interaction principle between the Homer EVH domain and RyR,[10–12] previous reports have rarely reported their dynamic recognition process.

Imaging ellipsometry has been developed from conventional ellipsometry.[13,14] It applies an expanded light beam and a CCD camera to replace the narrow light beam and the photodiode detector in the traditional ellipsometry setup. These improvements give imaging ellipsometry the advantages of ellipsometry and a microscope simultaneously. As a label-free characterization technique, imaging ellipsometry can detect a large area up to several square centimeters with high vertical resolution to sub-nanometer magnitude. Imaging ellipsometry has been proposed for inclusion in development of a biosensor to observe biomolecule interactions.[15,16] The biosensor based on imaging ellipsometry (BIE) comprises a micro-fluidic reactor and an imaging ellipsometry reader.[17] The micro-fluidic reactor injects different liquid solutions on the substrate to construct a patterned biomolecule microarray, while the imaging ellipsometry reader measures surface mass density distribution of the biomolecule microarray. As biomolecules interact, biomolecule complexes will be formed on the microarray surface, with resultant changes in surface mass density. By analyzing the surface mass density distribution, biomolecule interactions can be identified visually by imaging ellipsometry.[18] So far, BIE has been applied in biomedical and clinical detection, for example for five markers of hepatitis B virus,[19] tumor markers,[20] phage $M_{13}KO_7$,[21] severe acute respiratory syndrome virus,[22] and avian influenza virus.[23]

Conventionally, working under external reflection conditions, BIE cannot detect the dynamic process of biomolecule interactions because of fluid disturbance during solution delivery to the substrate. To overcome this disadvantage, a biosensor based on total internal reflection imaging ellipsometry (TIRIE)[24,25] has been proposed. Coupled with a micro-fluidic microarray reactor through a prism, TIRIE uses the evanescent wave on the interface under total internal reflection to detect biomolecule layer variation on the substrate. TIRIE biosensor not only exhibits high throughput and better sensitivity, but also can record *in situ* the whole process of biomolecule interactions in a series of images in grayscale. Thus, TIRIE can be used to form a real-time interaction curve and then deduce the binding affinity of biomolecule interactions.[26] TIRIE has been used in several biomedical applications for which conventional BIE was not sufficient for detection, for instance, identification of the weak interaction between tris and lysozyme.[27]

In this investigation, BIE is used to identify the specific interaction between Homer EVH domain and RyR, while TIRIE is introduced to measure their binding affinity.

[a]*NML, Institute of Mechanics, Chinese Academy of Sciences, 15 Bei-si-huan West Road, Beijing 100190, China. E-mail: gajin@imech.ac.cn; Fax: +86-10-82544138; +86-10-82544139; Tel: +86-10-82544138; +86-10-82544139*

[b]*Beijing Key Laboratory of Engineered Construction and Mechanobiology, Institute of Mechanics, Chinese Academy of Sciences, 15 Bei-si-huan West Road, Beijing 100190, China*

[c]*University of the Chinese Academy of Sciences, 19 Yu-quan Road, Beijing 100049, China*

[d]*Department of Biophysics, Peking University Health Science Center, Peking University, Beijing 100191, China*

Material and methods

Reagents

Aminopropyl-triethoxysilane (APTES), succinic anhydride, 1-(3-dimethylaminopropyl)-3-ethylcarbodiimidehydrochloride (EDC), *N*-hydroxyl-succinimide (NHS), 11-mercaptoundecanoic acid (MUA), human serum albumin (HSA), bovine serum albumin (BSA), rabbit immunoglobulin G and its antibody (IgG and anti-IgG) were purchased from Sigma-Aldrich. Binding buffer, Homer EVH type1 domain (EVH) and RyR type 1 (RyR) were provided by Professor Changcheng Yin's research group at the Medicine School of Peking University. The RyR was purified from 3-[(3-cholamidopropyl)dimethylammonio]-1-propanesulfonate solubilized skeletal sarcoplasmic reticulum, as described in previous articles.[28,29]

Detection procedure of EVH and RyR interaction with BIE

Silicon slices modified with APTES and succinic anhydride[18] were used as the BIE substrates to detect EVH and RyR interaction. After the substrate was placed in the micro-fluidic microarray reactor, 10 μL of a mixture solution of NHS (0.05 M) and EDC (0.2 M) were added by the micro-fluidic system at a flow rate of 2 μL min^{-1}. With NHS and EDC, carboxyl groups on the substrate can be activated to react with the amino group of the proteins. Subsequently, 10 μL EVH at concentration 0.1 mg mL^{-1} were delivered to the analytical cell to form a multiplex microarray biosensing surface at a flow rate of 1 μL min^{-1} for 10 min. To identify the EVH and RyR interaction specificity, 10 μL 0.1 mg mL^{-1} IgG were delivered to another cell. Then, 20 μL 0.05 mg mL^{-1} RyR and such negative controls as BSA, HSA and IgG were delivered at a flow rate of 2 μL min^{-1}. At the same time, RyR with the same concentration was added to the IgG modified surface as the blank control. As the interaction between IgG and anti-IgG is typical specific binding, 0.05 mg mL^{-1} anti-IgG was added to the IgG surface to verify the specificity between EVH and RyR. After rinsing with buffer and drying under nitrogen, the substrate was sampled by the imaging ellipsometry reader and its result was stored in images in grayscale.

Measuring the binding affinity between EVH and RyR with TIRIE

After modification with MUA ethanol solution (1 mM),[27] SF10 glass slides coated with 50 nm gold film were used as the TIRIE biosensor substrates. To activate the substrate surface, 10 μL of a mixture solution of NHS (0.05 M) and EDC (0.2 M) were added at a flow rate of 5 μL min^{-1}. After activation, EVH (0.15 mg mL^{-1}) was injected into each analytical area at a flow rate of 5 μL min^{-1} for 10 min. Then, excessive binding buffer was added to the EVH modified surface. RyR solutions diluted to different concentrations (10, 20, 40 and 80 μg mL^{-1}) and BSA as the negative control, (80 μg mL^{-1}) were delivered to the surface for 12 min. Eventually, binding buffer was injected for the surface rinsing. The whole process was visualized by TIRIE biosensor and recorded in a series of grayscale images with intervals of 0.2 seconds.

Results

Identification of EVH and RyR interaction with BIE

To identify the specific interaction between EVH and RyR, Fig. 1 shows the results in grayscale image and compares the values of the positive, the negative and the blank interactions. The grayscale value of each cell on the protein microarray reflects the surface mass concentration of protein layer proportionately.[15] The differences in grayscale value among these cells

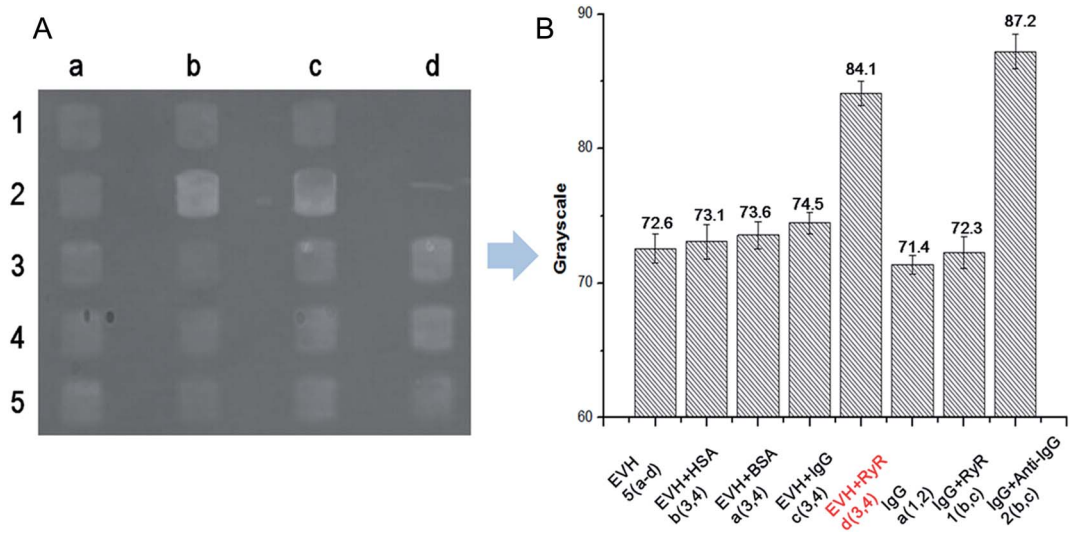

Fig. 1 Identification of EVH and RyR interaction with BIE. (A) The image in grayscale for EVH and RyR interaction detection. EVH is immobilized on rows 3–5 to form the sensing surface, while IgG as the blank control is bound on rows 1–2. Then, BSA, HSA and IgG as negative control and RyR are delivered to the following cells a(3, 4), b(3, 4), c(3, 4) and d(3, 4), respectively. Meanwhile, RyR and anti-IgG are injected to the blank control 1(b, c) and 2(b, c), respectively. (B) Histogram of grayscale values corresponding to (A).

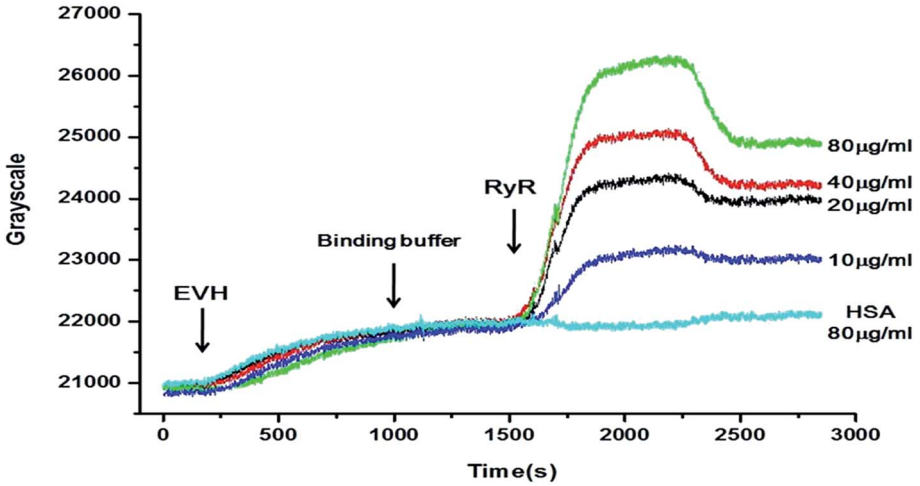

Fig. 2 Real-time curves of EVH and RyR interaction measured by TIRIE. EVH (150 μg mL^{-1}) is immobilized on the protein microarray, and then RyR at concentrations of 10 μg mL^{-1}, 20 μg mL^{-1}, 40 μg mL^{-1} and 80 μg mL^{-1} as well as HSA at a concentration of 80 μg mL^{-1} as the negative control were added to the EVH sensing surface.

indicate the surface mass concentration change caused by protein adsorption or binding. For blank controls, the grayscale value change is only about 0.9 before and after RyR injection. The grayscale value of negative controls goes up less than 1.9, whereas that of the cells where EVH interacts with RyR increases about 11.5, the same order as the IgG/anti-IgG interaction. Therefore, the remarkable increase in grayscale value for EVH and RyR binding cells confirms their specific interaction.

Binding affinity deduction of EVH and RyR interaction with TIRIE

To measure the binding affinity of EVH and RyR interaction, TIRIE was used to characterize their dynamic binding process. RyR with different concentrations and HSA as the negative control were injected to EVH surface and their interaction processes were recorded in real-time curves (shown in Fig. 2). For the negative controls, the tendency of the real-time curve remained stable with addition of HSA. However, the real-time curve increased sharply with injection of RyR at all the concentrations tested. With increasing RyR concentration, the grayscale value clearly increased, indicating the various binding amounts of EVH and RyR interaction.

The binding affinity of EVH and RyR interaction is given in eqn (1).[30,31]

$$R_{eq} = \frac{R_{max} C}{C + K_D} \quad (1)$$

where K_D describes the binding affinity in the biochemistry discipline, R_{eq} is the RyR binding amount at equilibrium, R_{max} is the maximum binding capacity of RyR on the EVH sensing surface and C is the RyR concentration in the analyte solution.

The binding data of the EVH and RyR interaction are plotted *versus* RyR concentration in Fig. 3. Origin 7.5 (OriginLab Corp.,

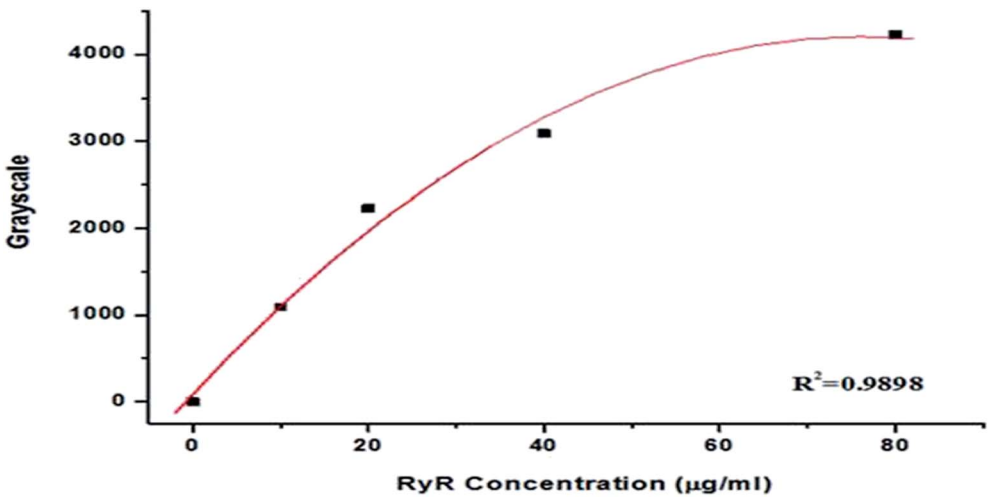

Fig. 3 Binding affinity deduction of EVH and RyR interaction.

MA, USA) was used to deduce the binding affinity of the EVH and RyR interaction through nonlinear regression analysis. The binding affinity of the EVH and RyR interaction was calculated to be 2.15×10^{-8} M, implying that the EVH and RyR interaction is a high-affinity interaction.[12]

Discussion

The interaction between the Homer EVH domain and RyR was identified by BIE and their binding affinity was deduced to 10^{-8} M by TIRIE. The results indicate that the interaction between the Homer EVH domain and RyR is relatively strong. Further analysis of the binding affinity between the Homer EVH domain and RyR will be helpful for understanding its role in intracellular calcium channels.

Acknowledgements

The authors acknowledge the financial support of the International Science & Technology Cooperation Program of China (2015DFG32390), the 7th Sino-Portugal Scientific and Technological Cooperation of 2013–2015, the National Basic Research Program of China (2015CB352100), and the National Natural Science Foundation of China (21305147) and (81472941).

References

1 M. Fill and J. A. Copello, Ryanodine receptor calcium release channels, *Physiol. Rev.*, 2002, **82**, 893–922.
2 R. Coronado, J. Morrissette, M. Sukhareva, *et al.*, Structure and function of ryanodine receptors, *Am. J. Physiol.*, 1994, **266**, 1485–1504.
3 L. Xu, J. P. Eu, G. Meissner, *et al.*, Activation of the cardiac calcium release channel (ryanodine receptor) by poly-*S*-nitrosylation, *Science*, 1998, **279**, 234–237.
4 S. Y. Hwang, J. Wei, J. H. Westhoff, R. S. Duncan, S. Qzawa, P. Volpe, K. Inokuchi and P. Koulen, Differential functional interaction of two Vesl/Homer protein isoforms with ryanodine receptor type 1: a novel mechanism for control of intracellular calcium signaling, *Cell Calcium*, 2003, **34**, 177–184.
5 D. M. Bers, Macromolecular complexes regulating cardiac ryanodine receptor function, *J. Mol. Cell. Cardiol.*, 2004, **37**, 417–429.
6 S. Kawaguchi, S. Shoji, M. Sunamori, T. Furuichi and S. Kawano, The fundamental properties of Homer 1 in association with cardiac ryanodine receptor in mouse heart, *J. Evol. Med. Dent. Sci.*, 2007, **54**, 103–108.
7 S. Y. Yoko and F. Teiichi, The Homer family proteins, *Genome Biol.*, 2007, **8**, 206–211.
8 M. Salanova, P. Volpe and D. Blottner, Homer protein family regulation in skeletal muscle and neuromuscular adaptation, *IUBMB Life*, 2013, **65**, 769–776.
9 W. S. Dong, J. G. Lee, H. S. Youn, H. E. Soo and H. K. Do, Ryanodine receptor assembly: a novel systems biology approach to 3D mapping, *Prog. Biophys. Mol. Biol.*, 2011, **105**, 145–161.
10 W. Feng, J. C. Tu, P. S. Vernon, P. D. Allen, P. F. Worley and I. N. Pessah, Homer regulates gain of ryanodine receptor type 1 channel complex, *J. Biol. Chem.*, 2002, **277**, 44722–44730.
11 W. Feng, J. C. Tu, P. Pouliquin, E. Cabrales, X. H. Shen, A. Dulhunty, P. F. Worley, P. D. Allen and I. N. Pessah, Dynamic regulation of ryanodine receptor type 1 (RyR1) channel activity by Homer 1, *Cell Calcium*, 2008, **43**, 307–314.
12 P. Pierre and F. D. Angela, Homer and the ryanodine receptor, *Eur. Biophys. J.*, 2009, **39**, 91–102.
13 G. Jin, P. Tengvall, I. Lundstrom and H. A. Arwin, Biosensor concept based on imaging ellipsometry for visualization of biomolecular interactions, *Anal. Biochem.*, 1995, **232**, 69–72.
14 G. Jin, R. Jansson and H. Arwin, Imaging ellipsometry revisited: Developments for visualization of thin transparent layers on silicon substrates, *Rev. Sci. Instrum.*, 1996, **67**, 2930–2936.
15 Z. H. Wang, Y. H. Meng, P. Q. Ying, C. Qi and G. Jin, A label-free protein microfluidic array for parallel immunoassays, *Electrophoresis*, 2006, **27**, 4078–4085.
16 Y. Niu and G. Jin, Protein microarray biosensors based on imaging ellipsometry techniques and their applications, *Protein Cell*, 2011, **2**, 445–455.
17 G. Jin, *et al.*, Development of biosensor based on imaging ellipsometry and biomedical applications, *Thin Solid Films*, 2011, **519**, 2750–2757.
18 Y. Niu and G. Jin, Surface modification methods to improve behavior of biosensor based on imaging ellipsometry, *Appl. Surf. Sci.*, 2013, **281**, 84–88.
19 C. Qi, W. Zhu and Y. Niu, Detection of Hepatitis B markers using biosensor based on imaging ellipsometry, *J. Viral Hepatitis*, 2009, **16**, 822–832.
20 Y. Niu, T. F. Kang and G. Jin, Joint detection of tumor markers with imaging ellipsometry biosensor, *Thin Solid Films*, 2014, **571**, 453–462.
21 C. Qi, Y. Lin, J. Feng, *et al.*, Phage $M_{13}KO_7$ detection with biosensor based on imaging ellipsometry and AFM microscopic confirmation, *Virus Res.*, 2009, **140**, 79–84.
22 C. Qi, J. Z. Duan, Z. H. Wang, *et al.*, Investigation of interaction between two neutralizing monoclonal antibodies and SARS virus using biosensor based on imaging ellipsometry, *Biomed. Microdevices*, 2006, **8**, 247–253.
23 C. Qi, X. S. Tian, S. Chen, *et al.*, Detection of avian influenza virus subtype H5 using a biosensor based on imaging ellipsometry, *Biosens. Bioelectron.*, 2010, **25**, 1530–1534.
24 Y. Y. Chen, Z. H. Wang, Y. H. Meng and G. Jin, Biosensor with total internal reflection imaging ellipsometry, *Int. J. Nanotechnol.*, 2007, **4**, 171–178.
25 Y. Y. Chen, Y. H. Meng and G. Jin, Optimization of off-null ellipsometry for air/solid interfaces, *Appl. Opt.*, 2007, **46**, 8475–8481.
26 L. Liu, Y. Y. Chen and Y. H. Meng, Improvement for sensitivity of biosensor with total internal reflection imaging ellipsometry (TIRIE), *Thin Solid Films*, 2011, **519**, 2758–2762.

27 T. F. Kang, Y. Niu and G. Jin, Visualization of the interaction between tris and lysozyme with a biosensor based on total internal reflection imaging ellipsometry, *Thin Solid Films*, 2014, **571**, 463–467.

28 M. Inui, A. Saito and S. Fleischer, Purification of the ryanodine receptor and identity with feet structures of junctional terminal cisternae of sarcoplasmic reticulum from fast skeletal muscle, *J. Biol. Chem.*, 1987, **262**, 1740–1747.

29 C. C. Yin and F. A. Lai, Intrinsic lattice formation by the ryanodine receptor calcium-release channel, *Nat. Cell Biol.*, 2005, **2**, 669–674.

30 X. Liu, *et al.*, Determination of affinities and antigenic epitopes of bovine cardiac troponin I (cTnI) with monoclonal antibodies by surface plasmon resonance biosensor, *Anal. Biochem.*, 2003, **314**, 301–309.

31 T. Fischer, M. Beyermann and K. W. Koch, Application of Different Surface Plasmon Resonance Biosensor Chips to Monitor the Interaction of the CaM-Binding Site of Nitric Oxide Synthase I and Calmodulin, *Biochem. Biophys. Res. Commun.*, 2001, **285**, 463–469.